

1 Early winter barium excess in the Southern Indian Ocean as an 2 annual remineralisation proxy (GEOTRACES GIPr07 cruise)

3 Natasha René van Horsten^{1,2,3}, Hélène Planquette¹, Géraldine Sarthou¹, Thomas James Ryan-Keogh²,
4 Nolwenn Lemaitre⁵, Thato Nicholas Mtshali⁴, Alakendra Roychoudhury³, and Eva Bucciarelli¹

5 ¹Univ Brest, CNRS, IRD, Ifremer, LEMAR, F-29280 Plouzane, France.

6 ²SOCCO, CSIR, Lower Hope road, Cape Town, South Africa, 7700.

7 ³TracEx, Department of Earth Sciences, Stellenbosch University, Stellenbosch, South Africa, 7600.

8 ⁴Department of Environment, Forestry and Fisheries, Oceans and Coast, Foretrust Building, Martin Hammerschlag Way, Cape
9 Town, South Africa, 8001

10 ⁵Department of Earth Sciences, Institute of Geochemistry and Petrology, ETH Zurich, Zurich, Switzerland.

11 *Correspondence to:* Natasha van Horsten (nvhorsten@csir.co.za), Eva Bucciarelli (Eva.Bucciarelli@univ-brest.fr)

12 **Abstract.** The Southern Ocean (SO) is of global importance to the carbon cycle, and processes such as mesopelagic
13 remineralisation that impact the efficiency of the biological carbon pump in this region need to be better constrained. During
14 this study early austral winter barium excess (Ba_{xs}) concentrations were measured for the first time, along 30°E in the Southern
15 Indian Ocean. Winter Ba_{xs} concentrations of 59 to 684 pmol L⁻¹ were comparable to those observed throughout other seasons.
16 The expected decline of the mesopelagic Ba_{xs} signal to background values during winter was not observed, supporting the
17 hypothesis that this remineralisation proxy likely has a longer timescale than previously reported. A compilation of available
18 SO mesopelagic Ba_{xs} data, including data from this study, shows an accumulation rate of $\sim 0.9 \mu\text{mol m}^{-2} \text{ d}^{-1}$ from September
19 to July that correlates with temporally integrated remotely sensed primary productivity (PP), throughout the SO from data
20 spanning ~ 20 years, advocating for a possible annual timescale of this proxy. The percentage of mesopelagic POC
21 remineralisation as calculated from estimated POC remineralisation fluxes over integrated remotely sensed PP was ~ 2 fold
22 higher south of the polar front ($19 \pm 15 \%$, $n = 39$) than north of the polar front ($10 \pm 10 \%$, $n = 29$), revealing the higher
23 surface carbon export efficiency further south. By linking integrated remotely sensed PP to mesopelagic Ba_{xs} stock we could
24 obtain better estimates of carbon export and remineralisation signals within the SO on annual and basin scales.

25 1 Introduction

26 The Southern Ocean (SO) is a carbon sink of global significance responsible for 40 – 50 % of the global oceans' carbon uptake
27 (Friedlingstein et al., 2019; Gregor et al., 2019; Gruber et al., 2019). Oceanic carbon uptake is regulated by various processes,
28 including the biological carbon pump (BCP). Inorganic carbon is consumed and released by photosynthetic organisms through
29 photosynthesis and respiration (Sarmiento and Gruber, 2006), thereby regulating the earth's carbon cycle by partially

30 sequestering photosynthetically fixed CO₂ in the ocean interior (Honjo et al., 2014). In particular, the SO BCP is a crucial
31 contributor to the earth's carbon cycle by exporting, from surface waters, ~ 3 Pg C yr⁻¹ of the ~ 10 Pg C yr⁻¹ global export
32 production (Schlitzer, 2002). The efficiency of the BCP is linked to the export and preservation of surface particulate matter
33 and is directly linked to atmospheric CO₂ levels, on glacial-interglacial timescales (Honjo et al., 2014; Sigman et al., 2010).
34 Sedimentation out of the surface layer (~ 100 m) is defined as surface export and out of the mesopelagic zone (~ 1000 m) as
35 deep export (Passow and Carlow, 2012). There are large gaps in our knowledge with regard to deep carbon export, internal
36 cycling and the seasonality of these processes (Takahashi et al., 2012). The magnitude of deep carbon export is dependent on
37 the efficiency of mesopelagic remineralisation (Jacquet et al., 2015) which can balance or even exceed particulate organic
38 carbon (POC) surface export, especially later in the growing season, thereby limiting deep export (Buesseler and Boyd, 2009;
39 Cardinal et al., 2005; Jacquet et al., 2011, 2015; Lemaitre et al., 2018; Planchon et al., 2013). A possible explanation for
40 imbalances between surface export and mesopelagic processes can be lateral advection of surface waters with lower particle
41 export relative to the mesopelagic signal (Planchon et al., 2013). It is also possible that continued remineralisation of earlier
42 larger export fluxes is detected in the mesopelagic signal but not in the export fluxes of in situ observations (Planchon et al.,
43 2013). In addition to this, the efficiency of remineralisation is influenced by the size and composition of exported particles
44 (Rosengard et al., 2015; Twining et al., 2014) as well as the pathway by which these particles are transported downwards (e.g.,
45 eddy-subduction, active migration, sinking or mixing) from the surface mixed layer to the mesopelagic zone (Boyd et al., 2019;
46 Le Moigne, 2019), creating an intricate web of processes to disentangle. Mesopelagic remineralisation has also been shown to
47 be influenced by environmental factors, such as temperature, phytoplankton community structure and nutrient availability
48 (Bopp et al., 2013; Buesseler and Boyd, 2009). Indeed, nutrient limitation in surface waters limits export and consequently
49 mesopelagic remineralisation by promoting the shift to smaller phytoplankton assemblages that preferentially take up recycled
50 nutrients in the surface mixed layer (Planchon et al., 2013). Phytoplankton community composition exerts an important control
51 where diatoms are more efficiently exported, due to their large size and ballasting by biogenic silica, compared to smaller non-
52 diatom phytoplankton (Armstrong et al., 2009; Buesseler, 1998; Ducklow et al., 2001). Latitudinal trends in remineralisation
53 efficiency can also be linked to temperature-dependent heterotrophs that are responsible for remineralisation (DeVries and
54 Weber, 2017; Marsay et al., 2015). The mesopelagic layer is under-studied, especially in the high latitudes, and therefore these
55 processes are poorly constrained, despite their importance to global elemental cycles, including that of carbon (Le Moigne,
56 2019; Robinson et al., 2010).

57 Export and remineralisation tracers, such as ²³⁴Th/²³⁸U and apparent oxygen utilization (AOU), have been used to study
58 mesopelagic POC remineralisation fluxes (Buesseler et al., 2005; Planchon et al., 2013; Lemaitre et al., 2018). Surface export
59 is set by the deficit of ²³⁴Th activities over ²³⁸U activities, while remineralisation processes are reflected by ²³⁴Th/²³⁸U ratios
60 larger than 1 below the surface mixed layer integrating processes over a 2 to 3 week period (Buesseler et al., 2005; Planchon
61 et al., 2013). AOU is the depletion of oxygen (O₂) in the ocean interior relative to surface saturation, due to biological
62 respiration, when surface water masses are subducted. AOU is dependent on salinity and temperature and integrates
63 remineralisation on timescales of years to decades (Ito et al., 2004). Inaccuracies have, however, been detected with AOU as

64 a remineralisation proxy, specifically in high latitude areas, due to O₂ undersaturation as a consequence of large temperature
65 gradients (Ito et al., 2004).

66 Barium excess (Ba_{xs}) is another proxy utilized to yield estimates of mesopelagic POC remineralisation fluxes. It is defined as
67 the “biogenic” portion of particulate Barium (pBa) as barite crystals, formed by the decay of bio-aggregates below the surface
68 mixed layer (Bishop, 1988; Dehairs et al., 1980; Lam and Bishop, 2007; Legeleux and Reyss, 1996; van Beek et al., 2007). As
69 these crystals are released, a Ba_{xs} peak is formed within the mesopelagic zone which has been found to correlate to primary
70 production (PP), O₂ consumption and POC remineralisation (Dehairs et al., 1997). Depth-integrated rates of O₂ consumption
71 between the base of the mixed layer and 1000 m were estimated using an inverse 1-D advection-diffusion-consumption model
72 (Shopova et al., 1995) to develop a transfer function between the Ba_{xs} signal and the rate of surface POC export for subsequent
73 mesopelagic remineralisation (Dehairs et al., 1997). Strong correlations have been obtained between the well-established
74 export/remineralisation flux proxy ²³⁴Th and Ba_{xs}, during studies conducted in the SO and the North Atlantic, confirming the
75 validity of Ba_{xs} as a remineralisation proxy (Cardinal et al., 2005; Lemaître et al., 2018; Planchon et al., 2013). Estimates of
76 POC remineralisation fluxes, using the Ba_{xs} proxy, are directly influenced by the background signal of Ba_{xs}, after partial
77 dissolution and sedimentation from the previous bloom season. It can be thought of as “pre-formed Ba_{xs}”, defined as the
78 Ba_{residual} signal at zero O₂ consumption (Jacquet et al., 2015). Because studies conducted in spring and summer suggest that
79 the mesopelagic Ba_{xs} signal lasts between a few days to a few weeks (Dehairs et al., 1997; Cardinal et al., 2005; Jacquet et al.,
80 2007, 2008a), it is postulated that winter measurements should give the true SO Ba_{residual} value (Jacquet et al., 2008b, 2011).
81 In this context, as part of a GEOTRACES process study (GIpr07) of a transect along 30°E in the Southern Indian Ocean
82 (58.5°S to 41.0°S), we studied Ba_{xs} distributions during early austral winter (July 2017) to better constrain the SO Ba_{residual}
83 concentrations and the timescale of this proxy. To our knowledge these are the first reported wintertime values for this proxy
84 in the SO.

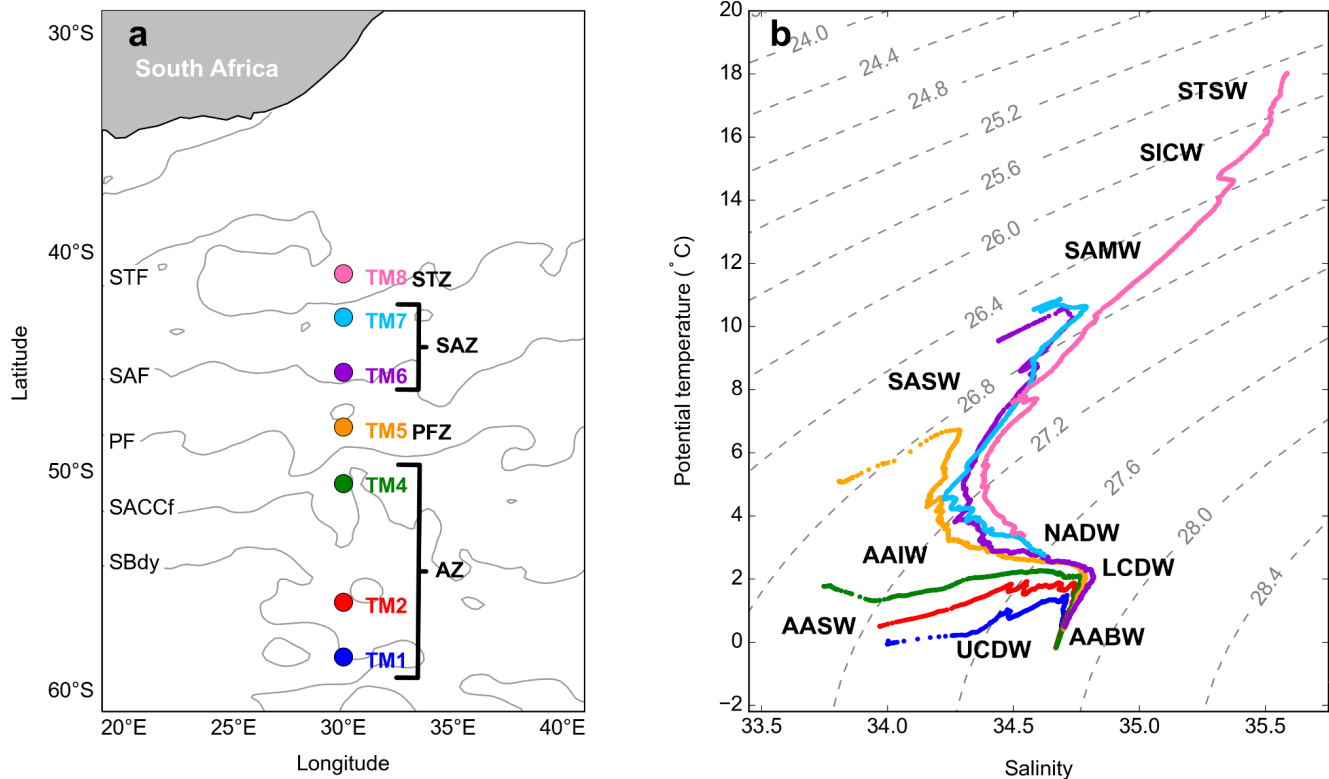
85 2 Materials and Methods

86 2.1 Sampling and hydrography

87 During the GEOTRACES GIpr07 cruise, which took place in early austral winter (28 June - 13 July 2017) onboard the R/V
88 *SA Agulhas II*, seven stations were sampled along 30°E, from 58.5°S to 41.0°S (WOCE I06S, Figure 1a). At each station
89 between 15 and 21 samples were collected from 25 m down to 1500 m, for shallow stations, and down to 4250 m, for deep
90 stations, to be analysed for multiple parameters.

91 Positions of the fronts during the cruise were determined using the July monthly mean absolute dynamic topography data from
92 the CLS/AVISO product (Rio et al., 2011), with boundary definitions from Swart et al. (2010). From north to south the
93 identified fronts are, the Subtropical Front (STF), the Subantarctic Front (SAF), the Polar Front (PF), the Southern Antarctic
94 Circumpolar Current Front (SACCf) and the Southern Boundary (SBdy) (Figure 1a). The marginal ice zone, identified as the

95 position of 30 % ice cover, was positioned at 61.7°S, approximately 3° (356 km) south of the southernmost station (de Jong et
96 al., 2018). Therefore, a potential sea ice influence on our study area can be disregarded.



97
98 **Figure 1:** (a) GEOTRACES GIPr07 cruise sampling stations overlaid on a map with frontal positions; namely, the Subtropical Front
99 (STF), the Subantarctic Front (SAF), the Polar Front (PF), the Southern Antarctic Circumpolar Current Front (SACCf) and the
00 Southern Boundary (SBdy), as determined by mean absolute dynamic topography (MADT) and crossing over four zones; namely,
01 the Antarctic zone (AZ), the Polar frontal zone (PFZ), the Subantarctic zone (SAZ) and the Subtropical zone (STZ). (b) Potential
02 temperature plotted against salinity, overlaid on isopycnals and identification of water masses sampled; namely, Subtropical Surface
03 Water (STSW), South Indian Central Water (SICW), Subantarctic Mode Water (SAMW), Subantarctic Surface Water (SASW),
04 Antarctic Intermediate Water (AAIW), Antarctic Surface Water (AASW), North Atlantic Deep Water (NADW), Lower
05 Circumpolar Deep Water (LCDW), Upper Circumpolar Deep Water (UCDW), and Antarctic Bottom Water (AABW).

06 2.2 Temperature, salinity and dissolved O₂

07 Temperature (°C), salinity and dissolved O₂ (μmol L⁻¹) profiles were measured by sensors (SBE 911plus) which were
08 calibrated by the manufacturer within a year prior to the cruise. At each cast, discrete seawater samples were collected and
09 analysed onboard for in situ calibration of sensor data for salinity (8410A Portasal salinometer, R² = 0.99) and dissolved O₂
10 concentrations (Metrohm 848 titrino plus, R² = 0.83; Ehrhardt et al., 1983). Temperature and salinity measurements were used
11 to calculate potential density (σ_0 ; Gill, 1982) to characterise water masses sampled and to identify the mixed layer depth
12 (MLD). The MLD is the depth at which there is a change of 0.03 kg m⁻³ in σ_0 from a near-surface value at ~ 10 m (de Boyer
13 Montégut, et al., 2004). Decreases in dissolved O₂ concentrations at intermediate depths, together with Ba_{xs} concentrations,
14 were used to define the mesopelagic remineralisation layer.

15 **2.3 pBa and pAl**

16 Profile sampling of the water column was conducted with a GEOTRACES compliant trace metal clean CTD housed on an
17 epoxy coated aluminium frame with titanium bolts equipped with 24 x 12 L trace metal clean Teflon coated GO-FLO bottles
18 (General Oceanics). All sampling and analyses were conducted following the GEOTRACES clean sampling and analysis
19 protocols (Cutter et al., 2017). Volumes of 2 to 7 L seawater were filtered from the GO-FLO bottles onto acid-washed
20 polyethersulfone filters (25 mm diameter, Supor, 0.45 μm pore size), for pBa and pAl analyses. Filters were mounted in-line
21 on the side spigot of each Go-Flo bottle, on swinnex filter holders. Furthermore, bottles were mixed 3 times before filtration,
22 as recommended by the GEOTRACES protocols (Cutter et al., 2017), to ensure homogenous sampling. Although the large
23 fast-sinking fraction of particles may be undersampled by using bottles (Bishop and Edmond, 1976; Planquette and Sherrell,
24 2012), comparing data that were generated using the same, internationally validated sampling systems and protocols (Cutter
25 et al. 2017), as we do in this study, minimises potential bias. After filtration, filters were placed in trace metal clean petri slides
26 (Pall) and kept frozen at -20°C until further processing on land. Sample processing was conducted under a class 100 HEPA
27 filtered laminar flow and extraction hood in a clean laboratory.

28 The pBa and pAl samples were processed and analysed 6 months after sample collection, at LEMAR (France). Unused blank
29 filters and filters containing the samples were acid reflux digested at 130°C in acid-cleaned savillex vials using a mixture of
30 HF and HNO₃ (both Ultrapure grade, Merck) solutions (Planquette and Sherrell, 2012). Archive solutions were stored in 3 ml
31 of 0.12 M HNO₃ (Ultrapur grade), of which 250 μL was diluted up to 2 mL for analysis by sector field inductively coupled
32 plasma mass spectrometry (SF-ICP-MS, Element XR Thermo Scientific). Samples were spiked with 1 $\mu\text{g L}^{-1}$ indium as an
33 internal standard to correct for instrument drift. The detection limits, defined as three times the standard deviation of the blanks
34 (unused filter blanks), were 0.39 pmol L^{-1} and 0.03 nmol L^{-1} ($n = 5$) for pBa and pAl, respectively. Mean amounts (in nmol)
35 of a given element determined in unused filter blanks were subtracted from the amounts in the sample filter then divided by
36 the volume filtered. Three certified reference materials (BCR 414, MESS 4 and PACS 3) were processed and analysed with
37 the samples to assess the accuracy of the methodology. Our values were in good agreement with the certified values of the
38 reference materials (Table 1) (Jochum et al., 2005). Percentage error of analyses was determined by the repeat analysis of
39 random samples during each run, the mean percentage error of sample analysis for pBa and pAl was 9.2 \pm 2.5 % and 11.1 \pm
40 4.6 % (mean \pm SD, $n = 6$), respectively.

41 **Table 1: Certified Reference Material recovery data for accuracy determination of pBa and pAl analyses**42 **N/A refers to instances where there are no certified values available to check for accuracy**

	pBa (mg/kg)	pAl (mg/kg)
PACS 3 certified (mean \pm SD)	N/A	65800 \pm 1700
PACS 3 measured (mean \pm SD)	N/A	73156 \pm 15416
PACS 3 mean % recovery	N/A	111 \pm 23

MESS 4 certified	920	79000 ± 2000
MESS 4 (mean ± SD)	1033 ± 28	100048 ± 26870
MESS 4 mean % recovery ± SD	112 ± 3	127 ± 34
BCR 414 indicative values	32 ± 5	2384 ± 652
BCR 414 (mean ± SD)	34 ± 4	2651 ± 317
BCR 414 mean % recovery ± SD	105 ± 12	111 ± 13

43

44

2.4 Ba_{xs} as a proxy for mesopelagic POC remineralisation

45 The non-lithogenic fraction of pBa, Ba_{xs}, was calculated by subtracting the lithogenic fraction of pBa from the total pBa
46 measured using Eq. 1. The lithogenic contribution to pBa was calculated by multiplying the pAl concentration with the Ba/Al
47 upper continental crust (UCC) ratio, 0.00135, as determined by Taylor and McLennan (1985).

48

49
$$Ba_{xs} = [pBa] - ([pAl] \times (Ba/Al)_{UCC}) \quad (1)$$

50

51 Total pBa and Ba_{xs} profiles were nearly identical with a mean percentage Ba_{xs} to total pBa of 99 ± 1 % (mean ± SD, n = 124;
52 Table S2), indicating that pBa from lithogenic sources was negligible. This ensures the accurate estimation of Ba_{xs}, which
53 requires that less than 50 % of pBa should be associated with lithogenic inputs (Dymond et al., 1992).

54 The mesopelagic POC remineralisation flux was estimated using Eq. 2 (Dehairs et al., 1997; Shopova et al., 1995).

55

56
$$Mesopelagic POC remineralisation = Z \times JO_2 \times (C:O_2)_{Redfield\ Ratio} \times 12.01 \quad (2)$$

57

58 Where the mesopelagic POC remineralisation flux is expressed in mg C m⁻² d⁻¹, Z is the depth range of the mesopelagic Ba_{xs}
59 layer (100 - 1000 m), C:O₂ is the stoichiometric molar ratio of carbon to O₂ consumption by remineralisation as per the Redfield
60 Ratio (127/175, Broecker et al., 1985), 12.01 is the molar mass of carbon (g mol⁻¹) and JO₂ is the rate of O₂ consumption (μmol
61 L⁻¹ d⁻¹) as estimated using Eq. 3 (Dehairs et al., 1997; Shopova et al., 1995).

62

63
$$JO_2 = (Mesopelagic\ Ba_{xs} - Ba_{residual})/17200 \quad (3)$$

64

65 Where mesopelagic Ba_{xs} is the depth-weighted average Ba_{xs} of the mesopelagic zone (pmol L⁻¹), the constant value of 17200
66 is the slope of the linear regression of depth-weighted average Ba_{xs} (pmol L⁻¹) versus O₂ consumption rate (μmol L⁻¹ d⁻¹) using
67 the Southern Ocean transfer function by Dehairs et al. (1997) and Ba_{residual} is the deep ocean background value of Ba_{xs} at zero

68 oxygen consumption. The literature value of 180 pmol L⁻¹ was used as the Ba_{residual} value (Dehairs et al., 1997) in our
69 calculations.

70 The integrated mesopelagic Ba_{xs} stock (μmol m⁻²) over the mesopelagic layer (100 - 1000 m) was calculated from the depth-
71 weighted average Ba_{xs} in order to investigate the link between the accumulated mesopelagic signal and the corresponding
72 integrated remotely sensed primary productivity (PP).

73 2.5 Integrated remotely sensed PP

74 The integrated remotely sensed PP (mg C m⁻² d⁻¹) within the surface mixed layer was calculated using the CbPM algorithm
75 (Behrenfeld et al., 2005), which requires chlorophyll concentration (mg m⁻³), particulate backscatter (λ 443 nm, m⁻¹),
76 photosynthetically active radiation (PAR; μmol photons m⁻² d⁻¹) and the MLD (m). Ocean Colour-Climate Change Initiative
77 (OC-CCI) data (<https://esa-oceancolour-cci.org/>), which blends existing data streams into a coherent record, meeting the
78 quality requirements for climate assessment (Sathyendranath et al., 2019), were used for chlorophyll and particulate
79 backscatter. PAR was taken from GLOB colour (<http://www.globcolour.info/>), and the MLD was taken from the climatology
80 of de Boyer Montegut et al. (2004). The integrated remotely sensed PP data were regridded to 0.25° spatially, using bilinear
81 interpolation using the Python programming package xESMF (Zhuang, 2018), and averaged monthly. The area-averaged PP
82 was averaged over a 6 x 1° rectangular sample area, positioned 6° upstream longitudinally, and 1° latitudinally centred around
83 each sampled station (see discussion for details). In order to assess the validity of the remotely sensed PP data and demonstrate
84 no meridional bias across the SO, the percentage valid pixels was calculated for data north (90 ± 20 %; mean ± SD, n = 370)
85 and south (82 ± 29 % mean ± SD, n = 488) of the PF, revealing no bias.

86 2.6 Integrated % POC remineralised

87 The integrated remineralised POC (mg C m⁻²) was estimated by multiplying the POC remineralisation flux (mg C m⁻² d⁻¹), as
88 estimated using the Ba_{xs} proxy method, by the number of days over which the corresponding remotely sensed PP (mg C m⁻² d⁻¹)
89 was subsampled. The % POC remineralised was then estimated as the percentage of integrated remotely sensed PP (mg C
90 m⁻²) remineralised, assuming that the mesopelagic Ba_{xs} stock signal observed is due to the remineralisation of the integrated
91 surface PP signal.

92 2.7 Statistical analysis

93 For statistical analysis, the least squares regression method was applied for assessment of significant correlations (Barbur et
94 al., 1994). Significant differences between regions and regressions were tested using Welch's t-test, with an alpha of 0.05 (95
95 % confidence level) (Kokoska and Zwillinger, 2000).

96

3 Results

97

3.1 Hydrography

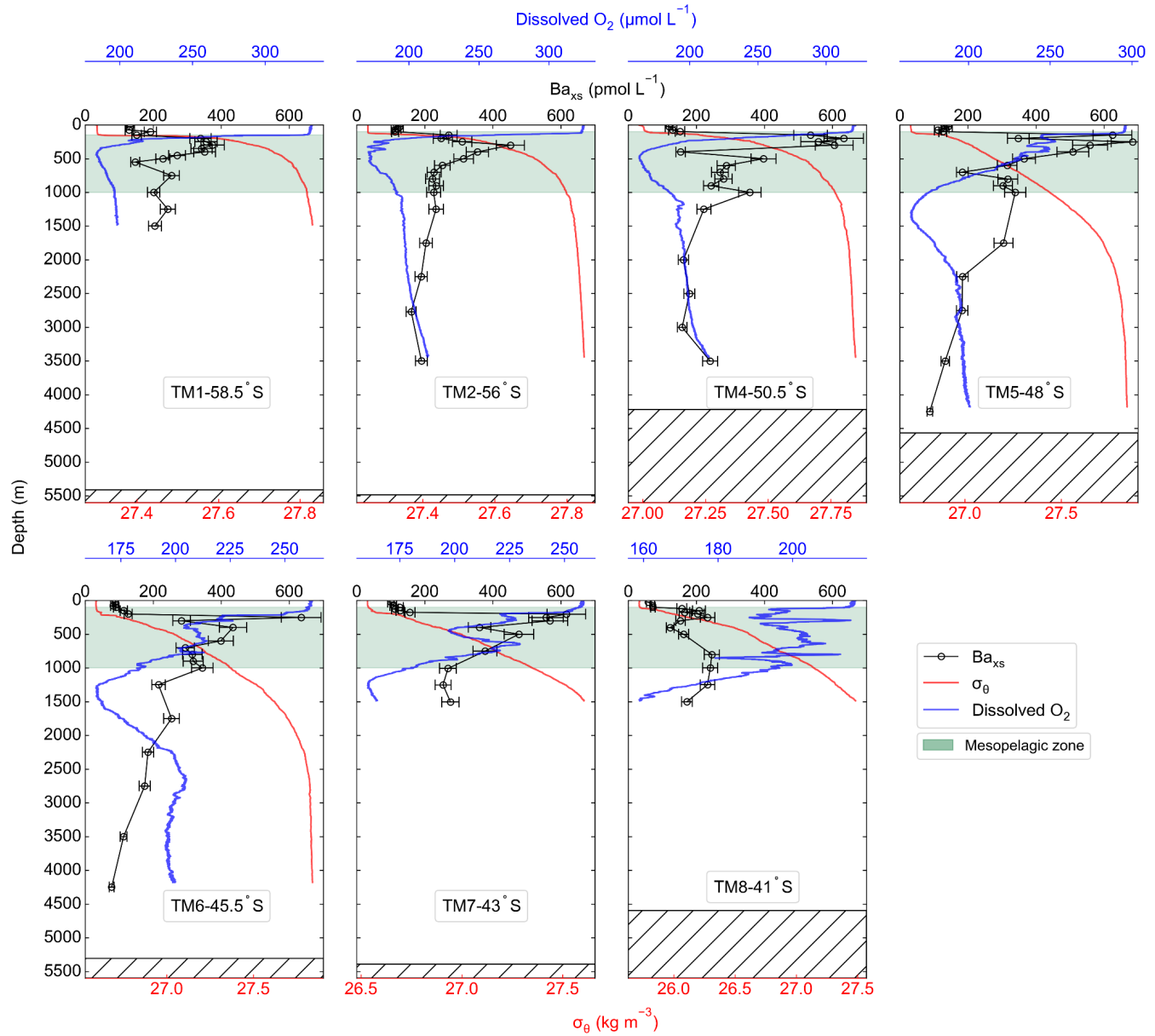
98 The potential temperature (θ) and salinity (S) along the transect ranged from -0.06 to 18.03 °C and from 33.77 to 35.59,
99 respectively. Where surface θ and S define four hydrographic zones; namely, the Antarctic zone (AZ; $\theta < 2.5$ °C; $S \leq 34$) from
00 ~ 50°S to 58.5°S, the polar frontal zone (PFZ; $\theta \cong 5$ °C; $S \cong 33.8$) at ~ 48°S, the subantarctic zone (SAZ; $5 < \theta < 11$ °C; 33.8
01 $< S < 34.7$) between 43°S and 45.5°S, and the subtropical zone (STZ; $\theta \geq 17.9$ °C; $S \cong 35.6$) at 41°S (Figure 1a; Anilkumar and
02 Sabu, 2017; Orsi et al., 1995; Pollard et al., 2002). The MLDs along the transect ranged between 97 and 215 m (144 ± 39 m;
03 mean \pm SD, $n = 7$), shoaling towards the PF (Table S1).

04 As can be observed on the T-S plot of stations sampled (Figure 1b), different water masses were sampled along the transect
05 throughout the water column. South of the polar front (SPF; $\gtrless 50$ °S; TM1, 2 and 4), from surface to depth, Antarctic Surface
06 Water (AASW; $27 < \sigma_\theta < 27.4$ kg.m⁻³), Upper and Lower Circumpolar Deep Water (UCDW; $27.2 < \sigma_\theta < 27.75$ kg.m⁻³ and
07 LCDW; $27.75 < \sigma_\theta < 27.85$ kg.m⁻³, respectively), and Antarctic Bottom Water (AABW; $27.8 < \sigma_\theta < 27.85$ kg.m⁻³) were
08 characterised. North of the polar front (NPF) and south of the STF (< 50 °S; TM5, 6 and 7), from surface to depth, Subantarctic
09 Surface Water (SASW; $26.5 < \sigma_\theta < 26.75$ kg.m⁻³), Antarctic Intermediate Water (AAIW; $26.7 < \sigma_\theta < 27.4$ kg.m⁻³), North
10 Atlantic Deep Water (NADW; $27 < \sigma_\theta < 27.85$ kg.m⁻³) and, as far north as 45.5°S, AABW close to the ocean floor, were
11 identified. At the northernmost station (TM8; 41°S), in the STZ, the water masses sampled include Subtropical Surface Water
12 (STSW; $\sigma_\theta \cong 25.7$ kg.m⁻³), South Indian Central Water (SICW; $25.8 < \sigma_\theta < 26.2$ kg.m⁻³), Subantarctic Mode Water (SAMW;
13 $26.2 < \sigma_\theta < 26.6$ kg.m⁻³), AAIW and NADW.

14

3.2 Dissolved O₂

15 The water column dissolved O₂ concentrations ranged from 159 to 333 μmol L⁻¹ (Figure 2). Maximum concentrations were
16 observed in the surface mixed layer, increasing southwards along the transect, with a mean value of 287 ± 40 μmol L⁻¹ (mean
17 \pm SD, $n = 700$). A decrease in concentrations below the MLD coincided with an increase in σ_θ . South of the PF, the decrease
18 in dissolved O₂ concentrations at the MLD was sharp and relatively shallow when compared to profiles NPF, which were more
19 gradual, spanning a wider depth range. Within the mesopelagic zone concentrations decreased down to 204 ± 29 μmol L⁻¹
20 (mean \pm SD, $n = 6373$), then remained relatively uniform below 1000 m at 192 ± 113 μmol L⁻¹ (mean \pm SD, $n = 12950$).



21
22 **Figure 2:** Ba_{xs} (black circles) with error bars, potential density (σ_{θ} ; red) and dissolved O_2 (blue) profiles sampled along the transect,
23 plotted against depth, for stations TM1 to TM8, from south to north. The green shaded area is the mesopelagic zone, and the hatched
24 area is the ocean floor.

25 **3.3 Ba_{xs} and estimated POC remineralisation fluxes**

26 Along the transect, Ba_{xs} concentrations ranged from 59 to 684 pmol L^{-1} . All profiles exhibited a depletion of Ba_{xs} in the upper
27 surface waters (59 - 152 pmol L^{-1}), then a rapid increase below the MLD (~ 150 m), with concentrations ranging between 113
28 and 684 pmol L^{-1} in the mesopelagic zone (100 - 1000 m, Figure 2). At the two southernmost stations (TM1 and TM2),

mesopelagic Ba_{xs} peaks spanned a narrower depth range (100 - 600 m) than stations further north, with concentrations reaching values of ~ 400 pmol L $^{-1}$. Concentrations were higher in the PFZ and SAZ with a maximum of 684 pmol L $^{-1}$ in the PFZ, at 48°S (TM5). The subsurface increase of Ba_{xs} started at slightly deeper depths (150 - 200 m) and spanned wider depth ranges down to 1000 m, at stations north of the PF. The STZ station, at 41°S (TM8), had the lowest concentrations, only increasing up to ~ 200 pmol L $^{-1}$. Double peaks were observed at all stations north of the PF, with a shallow and more substantial peak occurring in the upper mesopelagic zone and a second peak in the lower mesopelagic zone. Below the mesopelagic zone, Ba_{xs} concentrations decreased down to ~ 180 pmol L $^{-1}$ and remained relatively uniform.

The mean $Ba_{residual}$ concentration south of PF was 183 ± 29 pmol L $^{-1}$ (mean \pm SD, n = 7), whereas it was 142 ± 45 pmol L $^{-1}$ (mean \pm SD, n = 8) between the PF and the STF. The two regions were however not significantly different to each other when conducting a Welch's t-test (t-statistic = 2.10; p-value = 0.06) and when averaging all concentrations below 2000 m along the transect, the $Ba_{residual}$ concentration was 161 ± 43 pmol L $^{-1}$ (mean \pm SD, n = 15). This concentration is not statistically different from the literature value of 180 pmol L $^{-1}$ (Dehairs et al., 1997), which is widely used for estimates of POC remineralisation fluxes. For a better comparison with these previous estimates, we used 180 pmol L $^{-1}$ for the $Ba_{residual}$ concentration in our calculations.

The estimated POC remineralisation fluxes for the study area ranged from 6 to 96 mg C m $^{-2}$ d $^{-1}$ (Table S3), increasing northwards from the southernmost station up to the PFZ from 32 to 92 mg C m $^{-2}$ d $^{-1}$, then decreasing down to 70 mg C m $^{-2}$ d $^{-1}$ at the SAF. The highest flux was estimated in the SAZ, and the lowest flux was estimated in the STZ.

4 Discussion

4.1 Early wintertime Ba_{xs} and $Ba_{residual}$ concentrations

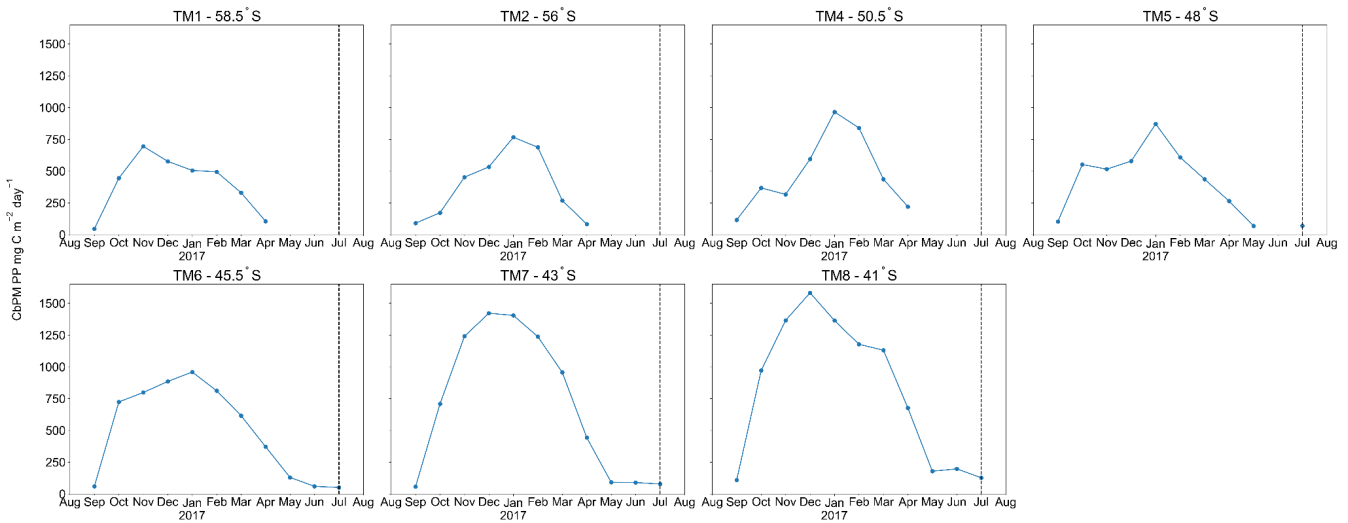
A noticeable difference between profiles sampled early in the bloom season (Dehairs et al., 1997; Jacquet et al., 2015) versus those sampled later (Cardinal et al., 2001; Planchon et al., 2013) is the contrasted Ba_{xs} concentrations in the surface mixed layer. Dehairs et al. (1997) has shown that these concentrations of Ba_{xs} can be as high as 9000 pmol L $^{-1}$ in areas of high productivity during spring, which then become depleted to concentrations below the SO $Ba_{residual}$ value of ~ 180 pmol L $^{-1}$, as productivity declines and surface POC export increases (Planchon et al., 2013). These high surface concentrations are, however, not due to the same process as the one that controls the Ba_{xs} concentrations within the mesopelagic zone (Jacquet et al., 2011). Surface water concentrations are associated with Ba adsorbed onto particles whereas the mesopelagic Ba_{xs} signal is due to barite crystals formed within decaying bio-aggregates (Cardinal et al., 2005; Lam and Bishop, 2007; Lemaitre et al., 2018; Sternberg et al., 2005). In this study, we observed surface depletion of Ba_{xs} at all stations, in line with the assumption that the bulk surface export from the preceding bloom had been achieved at the time of sampling and, the majority of the Ba_{xs} had been transferred to the mesopelagic zone.

A sharp increase in σ_0 observed at the MLD has previously been identified as the depth at which decaying bio-aggregates are formed (Lam and Bishop, 2007). These increases coincided with an increase in Ba_{xs} (Figure 2), linking the subsurface Ba_{xs}

61 signal to decaying bio-aggregates as per previous studies (Cardinal et al., 2005; Dehairs et al., 1997; Jacquet et al., 2011).
62 Additionally, decreases observed in dissolved O₂ profiles along the transect were also accompanied by coinciding increases in
63 Ba_{xs}, in line with O₂ consumption due to remineralisation within the mesopelagic zone (Figure 2) (Cardinal et al., 2005; Jacquet
64 et al., 2005, 2011). The observed range of mesopelagic Ba_{xs} concentrations (113 - 684 pmol L⁻¹) were comparable to those
65 previously reported in SO open waters (~ 200 - 1000 pmol L⁻¹; Cardinal et al., 2001, 2005; Jacquet et al., 2005, 2008a, 2008b,
66 2011, 2015; Planchon et al., 2013).

67 Ba_{xs} profiles exhibited similar distributions to those reported throughout bloom seasons in the SO, with distinct peaks observed
68 within the mesopelagic zone at all stations. Earlier in the bloom season, peaks mostly occur within the upper half of the
69 mesopelagic zone (100 - 500 m: Cardinal et al., 2001, 2005; Jacquet et al., 2005, 2008a, 2011, 2015), but as the season
70 progresses, they deepen down towards the bottom half of the mesopelagic zone (500 - >1000 m: Jacquet et al., 2008b, Planchon
71 et al., 2013). Deepening and widening of the remineralisation depth range can be expected as the season progresses, due to
72 continued remineralisation taking place as particles sink to the bottom of the mesopelagic zone (Lemaitre et al., 2018; Planchon
73 et al., 2013). This is also what we observed during early winter at stations NPF, with a second peak in deeper waters, as
74 observed by Jacquet et al. (2008b) during the iron (Fe) fertilisation experiment (EIFEX). The deeper peak could also be linked
75 to relatively larger cells that sink faster as they remineralise, possibly a large bloom earlier in the season.

76 A distinct latitudinal trend in mesopelagic depth-weighted average Ba_{xs} has generally been observed in the SO with the highest
77 values in the PFZ, decreasing north and southwards from the PF. These latitudinal trends tend to be accompanied by a
78 coinciding trend in in situ surface biomass measurements (Cardinal et al., 2005; Dehairs et al., 1997, Jacquet et al., 2011;
79 Planchon et al., 2013). During our early winter study, we observed a similar latitudinal trend in mesopelagic Ba_{xs} stock (μmol
80 m⁻²), with an increase from the southernmost station up to the PF, then varying around a maximum in the SAZ, down to the
81 lowest value in the STZ, whereas temporally integrated remotely sensed PP increased progressively northwards to a maximum
82 in the STZ (Figure S1). Time of sampling and extended blooms, which are characteristic of the SAZ (Thomalla et al., 2011),
83 could be contributing factors to the higher values observed in PP and mesopelagic Ba_{xs} distributions at stations north of the PF
84 (Figure S1). Contrary to what was expected, the profiles observed during our early winter study still show a significant
85 mesopelagic remineralisation signal, well after the summer bloom termination, which occurred between April and May (Figure
86 3), as defined by the point in time when community losses outweigh the growth rate (Thomalla et al., 2011).



87
88 **Figure 3: Time series, area-averaged (6 x 1° rectangular sample area, positioned 6° upstream longitudinally, and 1° latitudinally**

90 centred around each station) remotely sensed CbPM-PP (mg C m⁻² day⁻¹), monthly average from 08/2016 to 08/2017, dashed vertical lines indicate sampling date.

91 In deeper waters along the transect, south of the STF, (below 2000 m) where remineralisation is minimal compared to the
92 mesopelagic zone, our Ba_{xs} concentration of $161 \pm 43 \text{ pmol L}^{-1}$ (mean \pm SD, $n = 15$) is not significantly different from the
93 widely used Ba_{residual} concentration of 180 pmol L^{-1} , measured during early Spring to late Summer (e.g., Dehairs et al. 1997;
94 Jacquet et al., 2015; Planchon et al., 2013). We thus did not observe a wintertime decline to an expected “true” SO background
95 value, when PP and bacterial activity are suspected to be minimal (Jacquet et al., 2011). There are two possible explanations
96 for this; firstly, the decline to a winter background signal might never be achieved due to ongoing barite precipitation and
97 remineralisation, as well as the release of labile Ba attached to phytoplankton as they decay, precipitating into barite crystals,
98 which could possibly continue throughout winter (Cardinal et al., 2005). Secondly, the low sinking speed of suspended barite
99 ($\sim 0.3 \text{ m d}^{-1}$, Sternberg et al., 2008), once produced in the mesopelagic layer, implies that it would take ~ 6 years (not
00 considering reaggregation and redissolution) to sink from 300 m (\sim peak of production) to the bottom of the mesopelagic layer
01 (1000 m depth). The “true” background value may thus have to be measured at the very end of winter just before the initiation
02 of the spring bloom. This also suggests that the Ba_{xs} signal in the mesopelagic layer may represent remineralisation activity
03 over more than a few days to weeks, per previous reports (e.g., Dehairs et al., 1997; Jacquet et al., 2015; Planchon et al., 2013).

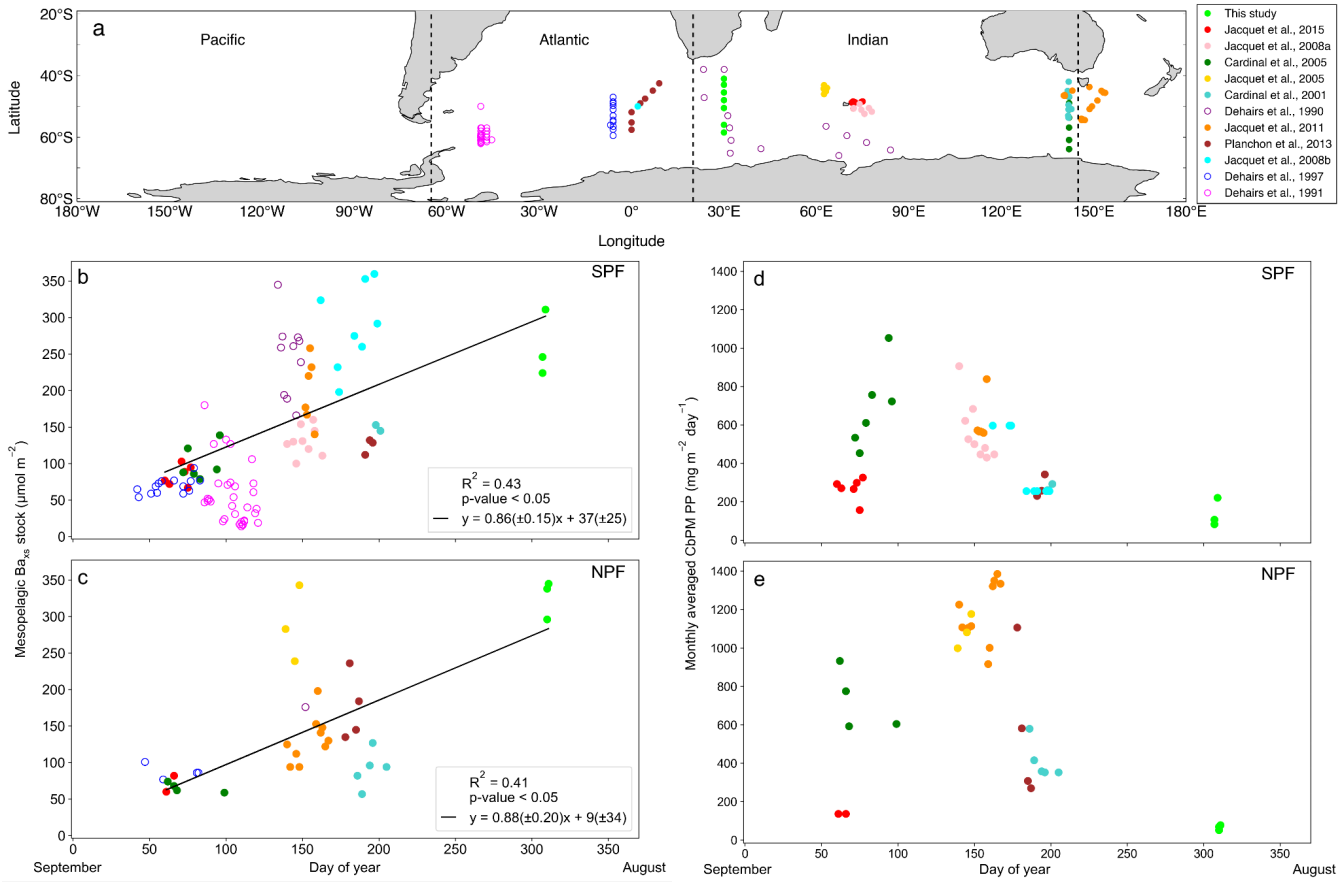
04 4.2 Timescale of the mesopelagic Ba_{xs} signal

05 The Ba_{xs} signal that we observed in winter is in agreement with the suggestion by Dehairs et al. (1997), that there can be
06 significant carry over between bloom seasons. Other studies have also pointed out that the timescale of this proxy is longer
07 than a snapshot view (Cardinal et al., 2005) and have highlighted a seasonal increase in mesopelagic Ba_{xs} (Jacquet et al., 2011).
08 This strongly suggests that the Ba_{xs} signal is not directly linked to synoptic measurements of PP at the time of sampling. In
09 order to investigate this hypothesis, for the first time, we compiled a SO mesopelagic Ba_{xs} stock dataset with all available

10 literature data including data from this study (Figure 4a, Table S3). The mesopelagic B_{xs} stock was integrated over the B_{xs}
11 peak depth range (as identified in each study). As can be seen on the map of the compilation dataset (Figure 4a), these data
12 points were collected across the three basins of the SO, over ~ 20 years. Despite this diversity in observations, a statistically
13 significant accumulation of mesopelagic B_{xs} with time is still observed, SPF (Figures 4b) and NPF (Figures 4c). Mesopelagic
14 B_{xs} accumulates at a rate of $0.86 (\pm 0.15) \mu\text{mol m}^{-2} \text{d}^{-1}$ SPF ($R^2 = 0.43$, p-value < 0.05, n = 43; Figure 4b), and at $0.88 (\pm 0.20)$
15 $\mu\text{mol m}^{-2} \text{d}^{-1}$ NPF ($R^2 = 0.41$, p-value < 0.05, n = 31; Figure 4c), with no statistically significant difference between the two
16 regions (Welch's t-test = 0.24; p-value = 0.80).

17 A possible link between the integrated mesopelagic B_{xs} stock and the corresponding integrated remotely sensed PP was
18 assessed for all studies conducted after September 1997, when remotely sensed PP data became available. To do so, we first
19 estimated that sub millimetre sized aggregates would take ~ 20 days to sink down to 1000 m (considered as the bottom of the
20 mesopelagic zone in this study), using a sinking speed of 50 m d^{-1} , that corresponds to an average literature value ($50 - 100 \text{ m}$
21 d^{-1} : Riebesell et al., 1991; $50 - 430 \text{ m d}^{-1}$ around South Georgia: Cavan et al. 2015; mean of $\sim 100 \text{ m d}^{-1}$ in the Southern Ocean
22 as reviewed in Laurenceau-Cornec et al., 2015; Marguerite Bay: $10 - 150 \text{ m d}^{-1}$: McDonnell and Buesseler, 2010). Assuming
23 a maximum surface current speed of 0.2 m s^{-1} (Ferrari and Nikurashin, 2010), it was estimated that these aggregates would
24 have originated, 346 km west from the station that was sampled for mesopelagic B_{xs} , ~ 20 days prior. Using this distance, the
25 dimensions of the sample area were set with the southernmost station (TM1) of this study, where degrees of longitude cover
26 the smallest area. For the sake of consistency this sample area was applied to all sampling locations of the considered dataset.
27 The integrated remotely sensed PP (see section 2.5) was then averaged spatially, positioned 6° upstream longitudinally, and
28 1° latitudinally centred around each station, in order to capture the surface PP that is assumed to translate to the mesopelagic
29 remineralisation and measured B_{xs} stock.

30 The monthly averaged remotely sensed PP, at the time of sampling, was compiled for the considered dataset, and we found
31 that the PP over the growing season (Figure 4d & e) reaches highest values between January and February (day 125 to 175 of
32 the year), thereafter, steadily decreasing to minimal values in July (\sim day 310 of the year, i.e., during our study). The
33 mesopelagic B_{xs} accumulation over time can, therefore, not be matched with the remotely sensed PP measured during the
34 month of sampling. A possible relationship between mesopelagic B_{xs} stock and temporally integrated remotely sensed PP
35 was further investigated by considering longer timescales. Remotely sensed PP of the preceding bloom was temporally
36 integrated from the preceding September, prior to sampling, as the start of the bloom, in general agreement with previous
37 bloom phenology studies (Thomalla et al., 2011), up to one month prior to the sampling date of the study, taking into
38 consideration time needed for export, aggregate formation and barite crystal release through remineralisation (~ 1 month).



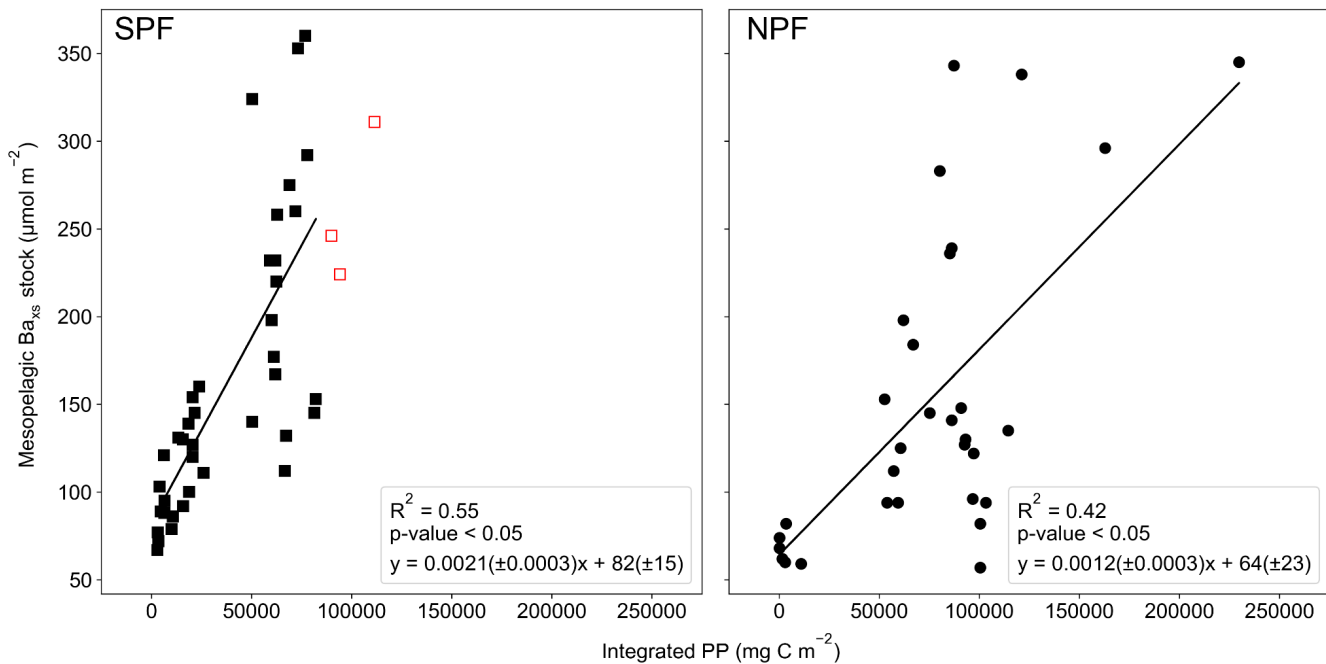
39

40 **Figure 4: (a)** Positions of Ba_{xs} observations compiled from all known SO studies, on a cylindrical equal-area projection of the SO,
41 the three SO basin cut offs are indicated by the dashed black lines, from left to right, Pacific, Atlantic and Indian. Integrated
42 mesopelagic Ba_{xs} stock plotted against day of year sampled, with the 1st of September set as day 1, for all available literature data
43 and winter data from this study. Data was split into two zones using the Polar Front (PF) to divide the SO; (b) South of the PF
44 (SPF) and (c) North of the PF (NPF). Monthly averaged remotely sensed PP plotted against day of year, for locations and dates of
45 the SO compilation dataset and winter data from this study; (d) SPF and (e) NPF. Open circles are data points from studies which
46 did not use HF in the particulate sample digestion procedure, regressions did not include these data points, there was, however, no
47 significant difference when including these data points (Table S3).

48 Varying timescales were considered between the preceding September up to 1 month prior to sampling (Sept - T1; Table S4),
49 in monthly increments, that could influence the relationship between remotely sensed PP and the mesopelagic Ba_{xs} stock (Table
50 S4). The strongest and most significant correlation between the mesopelagic Ba_{xs} stock and integrated remotely sensed PP, for
51 both north and south of the PF, was obtained from the preceding September up to 1 month prior to sampling (Table S4, Sept -
52 T1, SPF: Figure 5a, $R^2 = 0.55$, p-value < 0.05, n = 39; NPF: Figure 5b, $R^2 = 0.42$, p-value < 0.05, n = 31). When remote sensing
53 data was limited due to cloud cover and low sunlight during winter months, specifically at the southernmost stations, all
54 available data was used for the duration of the season. The correlation observed in the STZ is not significant at a 95 %
55 confidence level (p-value = 0.10); however, the limited number of data points (n = 6) may preclude any significance from

56 emerging. The significant positive correlations obtained south of the STF suggest that mesopelagic Ba_{xs} stock can be used as
 57 a remineralisation proxy on an annual timescale instead of only a few weeks. Figure 5 also reveals that for a given PP the
 58 mesopelagic Ba_{xs} stock was 2-fold higher SPF compared to NPF (Welch's t-test, t-statistic = 2.24; p-value < 0.05), this is
 59 further discussed below.

60



61

62 **Figure 5: Integrated mesopelagic Ba_{xs} stock plotted against integrated remotely sensed PP from the preceding September up to one**
 63 **month prior to sampling, all available literature data and winter data from this study, (a) South of the PF (SPF, black squares) and**
 64 **(b) North of the PF (NPF, black circles). Red open squares are data points from our winter dataset where there was not sufficient**
 65 **remote sensing PP data to integrate up to 1 month prior to sampling and available data up to 3 months prior to sampling was plotted**
 66 **but not included in the statistical analysis.**

67

4.3 Environmental factors influencing mesopelagic remineralisation and carbon export efficiency

68 Estimated POC remineralisation fluxes along the transect (6 - 96 mg C m⁻² d⁻¹) were on the upper end of the range of fluxes
 69 reported in previous studies, with the exception of the STZ station, but within the same order of magnitude for the SO as
 70 estimated from spring to autumn (0.2 - 118 mg C m⁻² d⁻¹; Table S3; Cardinal et al., 2005; Jacquet et al., 2011, 2015; Planchon
 71 et al., 2013). As the bloom season progresses, more efficient remineralisation rates have been reported in multiple studies
 72 (Cardinal et al., 2005; Jacquet et al., 2011; Planchon et al., 2013). However, during late summer as the bloom declines,
 73 observations indicate an inefficient BCP due to enhanced surface nutrient recycling (Dehairs et al., 1992; Jacquet et al., 2011;
 74 Planchon et al., 2013), leading to a decrease in surface POC export (Planchon et al., 2013). Seasonal variation is reported to
 75 be more pronounced northwards within the SO with the least variation observed in the southern Antarctic circumpolar current
 76 (Dehairs et al., 1997; Planchon et al., 2013).

77 The percentage of mesopelagic POC remineralisation as calculated from estimated POC remineralisation fluxes over integrated
78 remotely sensed PP, for the SO compilation dataset (SPF; $19 \pm 15 \%$, $n = 39$ and NPF; $10 \pm 10 \%$, $n = 29$; mean \pm SD; t-
79 statistic = 2.75; p-value <0.05 ; Table S3), was ~ 2 fold higher SPF than NPF, revealing the higher surface carbon export
80 efficiency SPF. Our estimates of % POC remineralised fall within the range of reported export efficiencies throughout the SO
81 (2 - 58 %; Jacquet et al., 2011; Morris et al., 2007; Savoye et al., 2008). Our values also support the inverse relationship
82 between export efficiency and productivity, with higher export efficiency in areas of lower production (HPLE; High
83 Productivity Low E-ratio, where e-ratio refers to the ratio between export production and net primary productivity, Fan et al.,
84 2020; Maiti et al., 2013). Estimated mesopelagic POC remineralisation has been reported to account for a significant fraction
85 of exported carbon in the PFZ and southwards, from 31 to 97 %, from spring to summer, whereas it only accounts for $\sim 50\%$
86 in the SAZ and SAF, during summer (Cardinal et al., 2005). A combination of variables can influence surface export efficiency
87 and the magnitude of the subsequent mesopelagic remineralisation, even more so when considering longer timescales. These
88 variables include physical dynamics and interlinked biogeochemical factors, i.e., bacterial activity, phytoplankton community
89 structure, zooplankton grazing and nutrient availability (Bopp et al., 2013; Buesseler and Boyd, 2009; Cardinal et al., 2005;
90 Jacquet et al., 2008b; Pyle et al., 2018). In previous studies, supply and loss via physical transport has been deemed negligible
91 relative to decay and loss via production, due to minimal advection and diffusion gradients observed on the timescale of days
92 to weeks. These processes were therefore assumed to have minimal impact on the mesopelagic signal (Dehairs et al., 1997;
93 Planchon et al., 2013; Rutgers van der Loeff et al., 2011). It has, however, been observed that features such as mesoscale
94 eddies can have an effect on B_{axs} distribution by influencing particle patterns on a broad spatial scale, homogenising
95 mesopelagic remineralisation signals by causing relatively flat profiles or shallower remineralisation peaks (Buesseler et al.,
96 2005; Jacquet et al., 2008b). The region of our winter study is known for being a mesoscale eddy hotspot due to the South-
97 West Indian Ridge (Ansorge et al., 2015). In the STZ, extremely dynamic submesoscale activity due to the Agulhas return
98 current may indeed have significantly influenced the mesopelagic signal, and may help explain the absence of correlation with
99 integrated surface PP. On the contrary, south of the STF, the significant correlations seem to indicate that physical transport
00 variability is not the main process affecting the mesopelagic B_{axs} signal, and that biogeochemical factors may be dominant.
01 The Fe-limited SAZ (Ryan-Keogh et al., 2018) and AZ (Viljoen et al., 2018) have generally mixed and seasonally changing
02 assemblages of pico-, nano- and micro-phytoplankton (Eriksen et al., 2018; Gall et al., 2001). Diatoms tend to dominate in the
03 silicate-rich waters south of the PF (Petrou et al., 2016; Rembauville et al., 2017; Wright et al., 2010), whilst seasonally silicate-
04 limited waters north of the PF, favour smaller phytoplankton groups (Freeman et al., 2018; Nissen et al., 2018; Trull et al.,
05 2018). HPLE regimes are indeed characteristic of large areas of the SAZ. They are mainly due to surface POC accumulation
06 caused by non-sinking particles, tending towards less efficient export of smaller cells (Fan et al., 2020). Even when large
07 particles are abundant in HPLE surface layers, a complex grazing community may prevent the export of large particles (Dehairs
08 et al., 1992; Lam and Bishop, 2007). This can explain the higher surface carbon export efficiency that we estimate SPF
09 compared to NPF. Export efficiency has also been linked to bacterial productivity with efficient surface remineralisation
10 limiting surface POC export, when most of the water column integrated bacterial productivity is restricted to the upper mixed

11 layer (Dehairs et al., 1992; Jacquet et al., 2011), which can be the case to varying degrees throughout the SO. In the STZ
12 phytoplankton communities are reported to be dominated by prokaryotic picoplankton including cyanobacteria and
13 prochlorophytes (Mendes et al., 2015). These groups utilise regenerated nutrients in the surface mixed layer tending towards
14 diminished surface export efficiency with high concentrations of non-sinking POC (Fan et al., 2020; Planchon et al. 2013). In
15 addition to this, the potential influence of high submesoscale activity, may explain the low mesopelagic Ba_{xs} measured at the
16 STZ station of this study, despite it being the station with the highest integrated PP (Figure S1). Linking temporally integrated
17 remotely sensed PP to mesopelagic Ba_{xs} stock, coupled with the added influence of physical dynamics affecting surface export
18 efficiencies, along longer timescales, could give better estimates of export and remineralisation signals throughout the SO, on
19 an annual and basin scale. Our estimates of percentage remineralised POC over remotely sensed PP may contribute to the
20 improved modelling of the C cycle over the SO, on an annual timescale.

21 5 Conclusions

22 Our unique early winter Ba_{xs} data were similar in magnitude and exhibited the same relationship with σ_0 and dissolved O_2
23 gradients as observed in summer, indicating that processes controlling this signal in summer are still driving the signal in early
24 winter. The expected decline of the mesopelagic Ba_{xs} signal to background values during winter was not observed in this study,
25 supporting the hypothesis that this remineralisation proxy likely has a longer timescale than previously reported. The absolute
26 decline might be delayed due to the cumulative behaviour of mesopelagic Ba_{xs} , ongoing remineralisation and barite
27 precipitation. The “true” SO background value may thus have to be measured at the very end of winter, prior to bloom initiation.
28 Significant positive correlations north and south of the PF, between mesopelagic Ba_{xs} stock and remotely sensed PP, integrated
29 from September to 1 month before sampling (Sept - T1), in combination with significant Ba_{xs} accumulation trends obtained
30 for the SO compilation dataset, suggest an annual timescale. They may also indicate that physical processes do not dominate
31 the mesopelagic signal on an annual scale, within the SO, and that biogeochemical factors are dominant. There is no significant
32 difference in mesopelagic Ba_{xs} and POC remineralisation, north and south of the PF, but the significantly higher integrated
33 remotely sensed PP to the north when compared to the south, indicates a greater export efficiency south of the PF. This is in
34 accordance with the phenomenon of HPLE regimes which are common throughout the SO, moreso north of the PF than south
35 of the PF (Fan et al., 2020). The longer timescale of Ba_{xs} and the cumulative behaviour of this proxy in the mesopelagic zone
36 make it possible to use Ba_{xs} on an annual scale for the estimation of POC remineralisation fluxes throughout the SO and to
37 better understand how variable environmental factors influence these processes on a basin scale. We believe that the
38 significance of these relationships will improve as more data become available (e.g., GEOTRACES IDP2021), which will
39 assist in better understanding and constraining the timescale of remineralisation and C export efficiency throughout the SO.

40 **6 Author contribution**

41 This study was conceptualised by N.R.vH, H.P, G.S and E.B. Formal analysis, investigation and validation of data was carried
42 out by N.R.vH, H.P, G.S, T.J.R-K and T.N.M. N.R.vH and T.J.R-K contributed towards the visualisation of the data. H.P,
43 G.S, T.N.M, A.R, N.L. and E.B contributed towards supervision and resources. Funding was acquired by N.R.vH, T.N.M, A.R
44 and E.B. All authors contributed towards writing, reviewing, and editing of the final manuscript.

45 **7 Acknowledgments**

46 This work was supported by the ISblue project, Interdisciplinary graduate school for the blue planet (ANR-17-EURE-0015)
47 and co-funded by a grant from the French government under the program "Investissements d'Avenir". International
48 collaboration was made possible by funding received by the French-South African National Research Foundation (NRF)
49 Collaboration (PROTEA; FSTR180418322331), NRF funding (SNA170518231343 and UID 110715) including funding from
50 South African Department of Science and Technology, French Ministry of National Education, Higher Education and
51 Research, and the French Ministry of Foreign Affairs and International Development. We would like to thank the captain and
52 crew of the R/V *SA Agulhas II* for their invaluable efforts, as well as all the research participants who assisted our fieldwork.
53 Thanks to Prof. I Ansorge, Dr M du Plessis and Dr E Portela for their assistance with water mass identification, and Dr C.
54 Jeandel for her invaluable expert insight.

55 **8 References**

56 Anilkumar, N. and Sabu, P.: Physical process influencing the ecosystem of the indian sector of southern ocean-An overview,
57 Proc. Indian Natl. Sci. Acad., 83(2), 363–376, doi:10.16943/ptinsa/2017/48960, 2017.

58 Ansorge, I. J., Jackson, J. M., Reid, K., Durgadoo, J. V., Swart, S. and Eberenz, S.: Evidence of a southward eddy corridor in
59 the South-West Indian ocean, Deep. Res. Part II Top. Stud. Oceanogr., 119, 69–76, doi:10.1016/j.dsr2.2014.05.012, 2015.

60 Armstrong, R. A., Peterson, M. L., Lee, C. and Wakeham, S. G.: Settling velocity spectra and the ballast ratio hypothesis,
61 Deep. Res. Part II Top. Stud. Oceanogr., 56(18), 1470–1478, doi:10.1016/j.dsr2.2008.11.032, 2009.

62 Barbur, V. A., Montgomery, D. C. and Peck, E. A.: Introduction to Linear Regression Analysis., Stat., 43(2), 339,
63 doi:10.2307/2348362, 1994.

64 Behrenfeld, M. J., Boss, E., Siegel, D. A. and Shea, D. M.: Carbon-based ocean productivity and phytoplankton physiology
65 from space, Global Biogeochem. Cycles, 19(1), 1–14, doi:10.1029/2004GB002299, 2005.

66 Bishop, J. K. B.: The barite-opal-organic carbon association in oceanic particulate matter, Nature, 332(6162), 341–343,
67 doi:10.1038/332341a0, 1988.

68 Bishop, J. K. B. and Edmond, J. M.: A new large volume filtration system for the sampling of oceanic particulate matter, J.
69 Mar. Res., 34, 181–198, 1976.

70 Bopp, L., Resplandy, L., Orr, J. C., Doney, S. C., Dunne, J. P., Gehlen, M., Halloran, P., Heinze, C., Ilyina, T., Séférian, R.,
71 Tjiputra, J. and Vichi, M.: Multiple stressors of ocean ecosystems in the 21st century: Projections with CMIP5 models,
72 Biogeosciences, 10(10), 6225–6245, doi:10.5194/bg-10-6225-2013, 2013.

73 Boyd, P. W., Claustre, H., Levy, M., Siegel, D. A. and Weber, T.: Multi-faceted particle pumps drive carbon sequestration in
74 the ocean, Nature, 568(7752), 327–335, doi:10.1038/s41586-019-1098-2, 2019.

75 Broecker, W. S., Takahashi, T. and Takahashi, T.: Sources and flow patterns of deep-ocean waters as deduced from potential
76 temperature, salinity, and initial phosphate concentration, J. Geophys. Res. Ocean., 90(C4), 6925–6939,
77 doi:10.1029/JC090iC04p06925, 1985.

78 Buesseler, K. O.: The decoupling of production and particulate export in the surface ocean, Global Biogeochem. Cycles, 12(2),
79 297–310, doi:10.1029/97GB03366, 1998.

80 Buesseler, K. O., Andrews, J. E., Pike, S. M., Charette, M. A., Goldson, L. E., Brzezinski, M. A. and Lance, V. P.: Particle
81 export during the Southern Ocean Iron Experiment (SOFeX), Limnol. Oceanogr., 50(1), 311–327,
82 doi:10.4319/lo.2005.50.1.0311, 2005.

83 Buesseler, K. O. and Boyd, P. W.: Shedding light on processes that control particle export and flux attenuation in the twilight
84 zone of the open ocean, Limnol. Oceanogr., 54(4), 1210–1232, doi:10.4319/lo.2009.54.4.1210, 2009.

85 Cardinal, D., Dehairs, F., Cattaldo, T. and André, L.: Geochemistry of suspended particles in the Subantarctic and Polar
86 Frontal zones south of Australia: Constraints on export and advection processes, J. Geophys. Res. Ocean., 106(C12),
87 31637–31656, doi:10.1029/2000JC000251, 2001.

88 Cardinal, D., Savoye, N., Trull, T. W., André, L., Kopczynska, E. E. and Dehairs, F.: Variations of carbon remineralisation in
89 the Southern Ocean illustrated by the Baxs proxy, Deep. Res. Part I Oceanogr. Res. Pap., 52(2), 355–370,
90 doi:10.1016/j.dsr.2004.10.002, 2005.

91 Cavan, E. L., Le Moigne, F. A. C., Poulton, A. J., Tarling, G. A., Ward, P., Daniels, C. J., Fragoso, G. M. and Sanders, R. J.:
92 Attenuation of particulate organic carbon flux in the Scotia Sea, Southern Ocean, is controlled by zooplankton fecal pellets,
93 Geophys. Res. Lett., 42(3), 821–830, doi:10.1002/2014GL062744, 2015.

94 Cutter, G., Casciotti, K., Croot, P., Geibert, W., Heimbürger, L.-E., Lohan, M., Planquette, H. and van de Flierdt, T.: Sampling
95 and Sample-handling Protocols for GEOTRACES Cruises. Version 3, 139pp. & Appendices [online] Available from:
96 <http://www.geotraces.org/images/stories/documents/intercalibration/Cookbook.pdf>, 2017.

97 de Boyer Montégut, C., Madec, G., Fischer, A. S., Lazar, A. and Iudicone, D.: Mixed layer depth over the global ocean: An
98 examination of profile data and a profile-based climatology, J. Geophys. Res. C Ocean., 109(12), 1–20,
99 doi:10.1029/2004JC002378, 2004.

00 Dehairs, F., Baeyens, W. and Goeyens, L.: Accumulation of Suspended Barite at Mesopelagic Depths and Export Production
01 in the Southern Ocean, Science (80-), 258(5086), 1332–1335, doi:10.1126/SCIENCE.258.5086.1332, 1992.

02 Dehairs, F., Chesselet, R. and Jedwab, J.: Discrete suspended particles of barite and the barium cycle in the open ocean, Earth
03 Planet. Sci. Lett., 49(2), 528–550, doi:10.1016/0012-821X(80)90094-1, 1980.

04 Dehairs, F., Goeyens, L., Stroobants, N., Bernard, P., Goyet, C., Poisson, A. and Chesselet, R.: On suspended barite and the
05 oxygen minimum in the Southern Ocean, *Global Biogeochem. Cycles*, 4(1), 85–102, doi:10.1029/GB004I001P00085,
06 1990.

07 Dehairs, F., Shopova, D., Ober, S., Veth, C. and Goeyens, L.: Particulate barium stocks and oxygen consumption in the
08 Southern Ocean mesopelagic water column during spring and early summer: Relationship with export production, *Deep.*
09 *Res. Part II Top. Stud. Oceanogr.*, 44(1–2), 497–516, doi:10.1016/S0967-0645(96)00072-0, 1997.

10 Dehairs, F., Stroobants, N. and Goeyens, L.: Suspended barite as a tracer of biological activity in the Southern Ocean, *Mar.*
11 *Chem.*, 35(1–4), 399–410, doi:10.1016/S0304-4203(09)90032-9, 1991.

12 de Jong, E., Vichi, M., Mehlmann, C. B., Eayrs, C., De Kock, W., Moldenhauer, M. and Audh, R. R.: Sea Ice conditions within
13 the Antarctic Marginal Ice Zone in winter 2017, onboard the SA Agulhas II., Univ. Cape Town, PANGAEA,
14 doi:<https://doi.org/10.1594/PANGAEA.885211>, 2018.

15 DeVries, T. and Weber, T.: The export and fate of organic matter in the ocean: New constraints from combining satellite and
16 oceanographic tracer observations, *Global Biogeochem. Cycles*, 31(3), 535–555, doi:10.1002/2016GB005551, 2017.

17 Ducklow, H. W., Steinberg, D. K. and Buesseler, K. O.: Upper ocean carbon export and the biological pump, *Oceanography*,
18 14(SPL.ISS. 4), 50–58, doi:10.5670/oceanog.2001.06, 2001.

19 Dymond, J., Suess, E. and Lyle, M.: Barium in Deep-Sea Sediment: A Geochemical Proxy for Paleoproductivity,
20 *Paleoceanography*, 7(2), 163–181, doi:10.1029/92PA00181, 1992.

21 Ehrhardt, M. (Manfred), Grasshoff, K., Kremling, K. (Klaus) and Almgren, T., Eds.: *Methods of seawater analysis / edited by*
22 *K. Grasshoff, M. Ehrhardt, K. Kremling; with contributions by T. Almgren ... [et al.], Verlag Chemie, Weinheim.*, 1983.

23 Eriksen, R., Trull, T. W., Davies, D., Jansen, P., Davidson, A. T., Westwood, K. and Van Den Enden, R.: Seasonal succession
24 of phytoplankton community structure from autonomous sampling at the Australian Southern Ocean Time Series (SOTS)
25 observatory, *Mar. Ecol. Prog. Ser.*, 589, 13–21, doi:10.3354/meps12420, 2018.

26 Fan, G., Han, Z., Ma, W., Chen, S., Chai, F., Mazloff, M. R., Pan, J. and Zhang, H.: Southern Ocean carbon export efficiency
27 in relation to temperature and primary productivity, *Sci. Rep.*, 10(1), 1–11, doi:10.1038/s41598-020-70417-z, 2020.

28 Ferrari, R. and Nikurashin, M.: Suppression of eddy diffusivity across jets in the Southern Ocean, *J. Phys. Oceanogr.*, 40(7),
29 1501–1519, doi:10.1175/2010JPO4278.1, 2010.

30 Freeman, N. M., Lovenduski, N. S., Munro, D. R., Krumhardt, K. M., Lindsay, K., Long, M. C. and Maclennan, M.: The
31 Variable and Changing Southern Ocean Silicate Front: Insights from the CESM Large Ensemble, *Global Biogeochem.*
32 *Cycles*, 32(5), 752–768, doi:10.1029/2017GB005816, 2018.

33 Friedlingstein, P., Jones, M. W., O’Sullivan, M., Andrew, R. M., Hauck, J., Peters, G. P., Peters, W., Pongratz, J., Sitch, S.,
34 Le Quéré, C., Bakker, D. C. E., Canadell, J. G., Ciais, P., Jackson, R. B., Anthoni, P., Barbero, L., Bastos, A., Bastrikov,
35 V., Becker, M., Bopp, L., Buitenhuis, E., Chandra, N., Chevallier, F., Chini, L. P., Currie, K. I., Feely, R. A., Gehlen, M.,
36 Gilfillan, D., Gkritzalis, T., Goll, D. S., Gruber, N., Gutekunst, S., Harris, I., Haverd, V., Houghton, R. A., Hurt, G., Ilyina,
37 T., Jain, A. K., Joetzer, E., Kaplan, J. O., Kato, E., Klein Goldewijk, K., Korsbakken, J. I., Landschützer, P., Lauvset, S.

38 K., Lefèvre, N., Lenton, A., Lienert, S., Lombardozzi, D., Marland, G., McGuire, P. C., Melton, J. R., Metzl, N., Munro,
39 D. R., Nabel, J. E. M. S., Nakaoka, S.-I., Neill, C., Omar, A. M., Ono, T., Pergon, A., Pierrot, D., Poulter, B., Rehder, G.,
40 Resplandy, L., Robertson, E., Rödenbeck, C., Séférian, R., Schwinger, J., Smith, N., Tans, P. P., Tian, H., Tilbrook, B.,
41 Tubiello, F. N., van der Werf, G. R., Wiltshire, A. J. and Zaehle, S.: Global Carbon Budget 2019, *Earth Syst. Sci. Data*,
42 11(4), 1783–1838, doi:10.5194/essd-11-1783-2019, 2019.

43 Gall, M. P., Boyd, P. W., Hall, J., Safi, K. A. and Chang, H.: Phytoplankton processes. Part 1: Community structure during
44 the Southern Ocean Iron RElease Experiment (SOIREE), *Deep. Res. Part II Top. Stud. Oceanogr.*, 48(11–12), 2551–2570,
45 doi:10.1016/S0967-0645(01)00008-X, 2001.

46 GEOTRACES Intermediate Data Product Group: The GEOTRACES Intermediate Data Product 2021 (IDP2021), NERC EDS
47 British Oceanographic Data Centre NOC, doi: 10.5285/cf2d9ba9-d51d-3b7c-e053-8486abc0f5fd, 2021.

48 Gill, A. E.: *Atmosphere-ocean dynamics*, NEW YORK, U.S.A., ACADEMIC PRESS INC., 1982.

49 Gregor, L., Lebehot, A. D., Kok, S. and Scheel Monteiro, P. M.: A comparative assessment of the uncertainties of global
50 surface ocean CO₂ estimates using a machine-learning ensemble (CSIR-ML6 version 2019a)-Have we hit the wall?,
51 *Geosci. Model Dev.*, 12(12), 5113–5136, doi:10.5194/gmd-12-5113-2019, 2019.

52 Gruber, N., Landschützer, P. and Lovenduski, N. S.: The variable southern ocean carbon sink, *Ann. Rev. Mar. Sci.*,
53 11(September), 159–186, doi:10.1146/annurev-marine-121916-063407, 2019.

54 Honjo, S., Eglington, T. I., Taylor, C. D., Ulmer, K. M., Sievert, S. M., Bracher, A., German, C. R., Edgcomb, V., Francois, R.,
55 Deboraiglesias-Rodriguez, M., Van Mooy, B. and Repeta, D. J.: Understanding the role of the biological pump in the global
56 carbon cycle: An imperative for ocean science, *Oceanography*, 27(3), 10–16, doi:10.5670/oceanog.2014.78, 2014.

57 Ito, T., Follows, M. J. and Boyle, E. A.: Is AOU a good measure of respiration in the oceans?, *Geophys. Res. Lett.*, 31(17), 1–
58 4, doi:10.1029/2004GL020900, 2004.

59 Jacquet, S. H. M., Dehairs, F., Cardinal, D., Navez, J. and Delille, B.: Barium distribution across the Southern Ocean frontal
60 system in the Crozet-Kerguelen Basin, *Mar. Chem.*, 95(3–4), 149–162, doi:10.1016/j.marchem.2004.09.002, 2005.

61 Jacquet, S. H. M., Dehairs, F., Dumont, I., Becquevort, S., Cavagna, A. J. and Cardinal, D.: Twilight zone organic carbon
62 remineralization in the Polar Front Zone and Subantarctic Zone south of Tasmania, *Deep. Res. Part II Top. Stud. Oceanogr.*,
63 58(21–22), 2222–2234, doi:10.1016/j.dsr2.2011.05.029, 2011.

64 Jacquet, S. H. M., Dehairs, F., Elskens, M., Savoye, N. and Cardinal, D.: Barium cycling along WOCE SR3 line in the Southern
65 Ocean, *Mar. Chem.*, 106(1-2 SPEC. ISS.), 33–45, doi:10.1016/j.marchem.2006.06.007, 2007.

66 Jacquet, S. H. M., Dehairs, F., Lefèvre, D., Cavagna, A. J., Planchon, F., Christaki, U., Monin, L., André, L., Closset, I. and
67 Cardinal, D.: Early spring mesopelagic carbon remineralization and transfer efficiency in the naturally iron-fertilized
68 Kerguelen area, *Biogeosciences*, 12(6), 1713–1731, doi:10.5194/bg-12-1713-2015, 2015.

69 Jacquet, S. H. M., Dehairs, F., Savoye, N., Obernosterer, I., Christaki, U., Monnin, C. and Cardinal, D.: Mesopelagic organic
70 carbon remineralization in the Kerguelen Plateau region tracked by biogenic particulate Ba, *Deep. Res. Part II Top. Stud. Oceanogr.*,
71 55(5–7), 868–879, doi:10.1016/j.dsr2.2007.12.038, 2008a.

72 Jacquet, S. H. M., Savoye, N., Dehairs, F., Strass, V. H. and Cardinal, D.: Mesopelagic carbon remineralization during the
73 European Iron Fertilization Experiment, *Global Biogeochem. Cycles*, 22(1), 1–9, doi:10.1029/2006GB002902, 2008b.

74 Jochum, K. P., Nohl, U., Herwig, K., Lammel, E., Stoll, B. and Hofmann, A. W.: GeoReM: A new geochemical database for
75 reference materials and isotopic standards, *Geostand. Geoanalytical Res.*, 29(3), 333–338, doi:10.1111/j.1751-
76 908x.2005.tb00904.x, 2005.

77 Kokoska, S. and Zwillinger, D.: *CRC Standard Probability and Statistics Tables and Formulae*, Student Edition., 2000.

78 Lam, P. J. and Bishop, J. K. B.: High biomass, low export regimes in the Southern Ocean, *Deep. Res. Part II Top. Stud.*
79 *Oceanogr.*, 54(5–7), 601–638, doi:10.1016/j.dsr2.2007.01.013, 2007.

80 Laurenceau-Cornec, E. C., Trull, T. W., Davies, D. M., Bray, S. G., Doran, J., Planchon, F., Carlotti, F., Jouandet, M. P.,
81 Cavagna, A. J., Waite, A. M. and Blain, S.: The relative importance of phytoplankton aggregates and zooplankton fecal
82 pellets to carbon export: Insights from free-drifting sediment trap deployments in naturally iron-fertilised waters near the
83 Kerguelen Plateau, *Biogeosciences*, 12(4), 1007–1027, doi:10.5194/BG-12-1007-2015, 2015.

84 Le Moigne, F. A. C.: Pathways of Organic Carbon Downward Transport by the Oceanic Biological Carbon Pump, *Front. Mar.*
85 *Sci.*, 6, doi:10.3389/fmars.2019.00634, 2019.

86 Legeleux, F. and Reyss, J. L.: $^{228}\text{Ra}/^{226}\text{Ra}$ activity ratio in oceanic settling particles: Implications regarding the use of barium
87 as a proxy for paleoproductivity reconstruction, *Deep. Res. Part I Oceanogr. Res. Pap.*, 43(11–12), 1857–1863,
88 doi:10.1016/S0967-0637(96)00086-6, 1996.

89 Lemaitre, N., Planquette, H., Planchon, F., Sarthou, G., Jacquet, S., García-Ibáñez, M. I., Gourain, A., Cheize, M., Monin, L.,
90 André, L., Laha, P., Terryn, H. and Dehairs, F.: Particulate barium tracing of significant mesopelagic carbon
91 remineralisation in the North Atlantic, *Biogeosciences*, 15(8), 2289–2307, doi:10.5194/bg-15-2289-2018, 2018.

92 Maiti, K., Charette, M. A., Buesseler, K. O. and Kahru, M.: An inverse relationship between production and export efficiency
93 in the Southern Ocean, *Geophys. Res. Lett.*, 40(8), 1557–1561, doi:10.1002/GRL.50219, 2013.

94 Marsay, C. M., Sanders, R. J., Henson, S. A., Pabortsava, K., Achterberg, E. P. and Lampitt, R. S.: Attenuation of sinking
95 particulate organic carbon flux through the mesopelagic ocean, *Proc. Natl. Acad. Sci. U. S. A.*, 112(4), 1089–1094,
96 doi:10.1073/pnas.1415311112, 2015.

97 McDonnell, A. M. P. and Buesseler, K. O.: Variability in the average sinking velocity of marine particles, *Limnol. Oceanogr.*,
98 55(5), 2085–2096, doi:10.4319/LO.2010.55.5.2085, 2010.

99 Mendes, C. R. B., Kerr, R., Tavano, V. M., Cavalheiro, F. A., Garcia, C. A. E., Gauns Dessai, D. R. and Anilkumar, N.: Cross-
00 front phytoplankton pigments and chemotaxonomic groups in the Indian sector of the Southern Ocean, *Deep. Res. Part II*
01 *Top. Stud. Oceanogr.*, 118, 221–232, doi:10.1016/j.dsr2.2015.01.003, 2015.

02 Morris, P. J., Sanders, R., Turnewitsch, R. and Thomalla, S.: ^{234}Th -derived particulate organic carbon export from an island-
03 induced phytoplankton bloom in the Southern Ocean, *Deep Sea Res. Part II Top. Stud. Oceanogr.*, 54(18–20), 2208–2232,
04 doi:10.1016/J.DSR2.2007.06.002, 2007.

05 Nissen, C., Vogt, M., Münnich, M., Gruber, N. and Haumann, F. A.: Factors controlling coccolithophore biogeography in the
06 Southern Ocean, *Biogeosciences*, 15(22), 6997–7024, doi:10.5194/bg-15-6997-2018, 2018.

07 Orsi, A. H., Whitworth, T. and Nowlin, W. D.: On the meridional extent and fronts of the Antarctic Circumpolar Current,
08 Deep. Res. Part I, 42(5), 641–673, doi:10.1016/0967-0637(95)00021-W, 1995.

09 Passow, U. and Carlson, C. A.: The biological pump in a high CO₂ world, *Mar. Ecol. Prog. Ser.*, 470(2), 249–271,
10 doi:10.3354/meps09985, 2012.

11 Petrou, K., Kranz, S. A., Trimborn, S., Hassler, C. S., Ameijeiras, S. B., Sackett, O., Ralph, P. J. and Davidson, A. T.: Southern
12 Ocean phytoplankton physiology in a changing climate, *J. Plant Physiol.*, 203, 135–150,
13 doi:<https://doi.org/10.1016/j.jplph.2016.05.004>, 2016.

14 Planchon, F., Cavagna, A. J., Cardinal, D., André, L. and Dehairs, F.: Late summer particulate organic carbon export and
15 twilight zone remineralisation in the Atlantic sector of the Southern Ocean, *Biogeosciences*, 10(2), 803–820,
16 doi:10.5194/bg-10-803-2013, 2013.

17 Planquette, H. and Sherrell, R. M.: Sampling for particulate trace element determination using water sampling bottles:
18 Methodology and comparison to in situ pumps, *Limnol. Oceanogr. Methods*, 10(5), 367–388,
19 doi:10.4319/lom.2012.10.367, 2012.

20 Pollard, R. T., Lucas, M. I. and Read, J. F.: Physical controls on biogeochemical zonation in the Southern Ocean, *Deep. Res.*
21 Part II Top. Stud. Oceanogr., 49(16), 3289–3305, doi:10.1016/S0967-0645(02)00084-X, 2002.

22 Pyle, K. M., Hendry, K. R., Sherrell, R. M., Legge, O., Hind, A. J., Bakker, D., Venables, H. and Meredith, M. P.: Oceanic
23 fronts control the distribution of dissolved barium in the Southern Ocean, *Mar. Chem.*, 204(July), 95–106,
24 doi:10.1016/j.marchem.2018.07.002, 2018.

25 Rembauville, M., Briggs, N., Ardyna, M., Uitz, J., Catala, P., Penkerc'h, C., Poteau, A., Claustre, H. and Blain, S.: Plankton
26 Assemblage Estimated with BGC-Argo Floats in the Southern Ocean: Implications for Seasonal Successions and Particle
27 Export, *J. Geophys. Res. Ocean.*, 122(10), 8278–8292, doi:10.1002/2017JC013067, 2017.

28 Riebesell, U.: Particle aggregation during a diatom bloom. II. Biological aspects, *Mar. Ecol. Prog. Ser.*, 69(3), 281–291,
29 doi:10.3354/meps069281, 1991.

30 Rio, M. H., Guinehut, S. and Larnicol, G.: New CNES-CLS09 global mean dynamic topography computed from the
31 combination of GRACE data, altimetry, and in situ measurements, *J. Geophys. Res. Ocean.*, 116(7), 1–25,
32 doi:10.1029/2010JC006505, 2011.

33 Robinson, C., Steinberg, D. K., Anderson, T. R., Arístegui, J., Carlson, C. A., Frost, J. R., Ghiglione, J. F., Hernández-León,
34 S., Jackson, G. A., Koppelman, R., Quéguiner, B., Ragueneau, O., Rassoulzadegan, F., Robison, B. H., Tamburini, C.,
35 Tanaka, T., Wishner, K. F. and Zhang, J.: Mesopelagic zone ecology and biogeochemistry - A synthesis, *Deep. Res. Part*
36 *II Top. Stud. Oceanogr.*, 57(16), 1504–1518, doi:10.1016/j.dsr2.2010.02.018, 2010.

37 Rosengard, S. Z., Lam, P. J., Balch, W. M., Auro, M. E., Pike, S., Drapeau, D. and Bowler, B.: Carbon export and transfer to
38 depth across the Southern Ocean Great Calcite Belt, *Biogeosciences*, 12(13), 3953–3971, doi:10.5194/bg-12-3953-2015,
39 2015.

40 Rutgers van der Loeff Michiel, M., Cai, P. H., Stimac, I., Bracher, A., Middag, R., Klunder, M. B. and van Heuven, S. M. A.
41 C.: 234Th in surface waters: Distribution of particle export flux across the Antarctic Circumpolar Current and in the
42 Weddell Sea during the GEOTRACES expedition ZERO and DRAKE, *Deep. Res. Part II Top. Stud. Oceanogr.*, 58(25–
43 26), 2749–2766, doi:10.1016/j.dsr2.2011.02.004, 2011.

44 Ryan-Keogh, T. J., Thomalla, S. J., Mtshali, T. N., Van Horsten, N. R. and Little, H. J.: Seasonal development of iron limitation
45 in the sub-Antarctic zone, *Biogeosciences*, 15(14), 4647–4660, doi:10.5194/bg-15-4647-2018, 2018.

46 Sarmiento, J., & Gruber, N. *Ocean Biogeochemical Dynamics*, Princeton University Press, Princeton, Oxford
47 doi:10.2307/j.ctt3fgxqx, 2006.

48 Sathyendranath, S., Brewin, R. J. W., Brockmann, C., Brotas, V., Calton, B., Chuprin, A., Cipollini, P., Couto, A. B., Dingle,
49 J., Doerffer, R., Donlon, C., Dowell, M., Farman, A., Grant, M., Groom, S., Horseman, A., Jackson, T., Krasemann, H.,
50 Lavender, S., Martinez-Vicente, V., Mazeran, C., Mélin, F., Moore, T. S., Müller, D., Regner, P., Roy, S., Steele, C. J.,
51 Steinmetz, F., Swinton, J., Taberner, M., Thompson, A., Valente, A., Zühlke, M., Brando, V. E., Feng, H., Feldman, G.,
52 Franz, B. A., Frouin, R., Gould, R. W., Hooker, S. B., Kahru, M., Kratzer, S., Mitchell, B. G., Muller-Karger, F. E., Sosik,
53 H. M., Voss, K. J., Werdell, J. and Platt, T.: An ocean-colour time series for use in climate studies: The experience of the
54 ocean-colour climate change initiative (OC-CCI), *Sensors (Switzerland)*, 19(19), doi:10.3390/s19194285, 2019.

55 Savoye, N., Trull, T. W., Jacquet, S. H. M., Navez, J. and Dehairs, F.: 234Th-based export fluxes during a natural iron
56 fertilization experiment in the Southern Ocean (KEOPS), *Deep Sea Res. Part II Top. Stud. Oceanogr.*, 55(5–7), 841–855,
57 doi:10.1016/J.DSR2.2007.12.036, 2008.

58 Schlitzer, R.: Carbon export fluxes in the Southern Ocean: Results from inverse modeling and comparison with satellite-based
59 estimates, *Deep. Res. Part II Top. Stud. Oceanogr.*, 49(9–10), 1623–1644, doi:10.1016/S0967-0645(02)00004-8, 2002.

60 Shopova, D., Dehairs, F. and Baeyens, W.: A simple model of biogeochemical element distribution in the oceanic water
61 column, *J. Mar. Syst.*, 6(4), 331–344, doi:10.1016/0924-7963(94)00032-7, 1995.

62 Sigman, D. M., Hain, M. P. and Haug, G. H.: The polar ocean and glacial cycles in atmospheric CO₂ concentration, *Nature*,
63 466(7302), 47–55, doi:10.1038/nature09149, 2010.

64 Sternberg, E., Jeandel, C., Robin, E. and Souhaut, M.: Seasonal cycle of suspended barite in the mediterranean sea, *Geochim.
65 Cosmochim. Acta*, 72(16), 4020–4034, doi:10.1016/J.GCA.2008.05.043, 2008.

66 Sternberg, E., Tang, D., Ho, T. Y., Jeandel, C. and Morel, F. M. M.: Barium uptake and adsorption in diatoms, *Geochim.
67 Cosmochim. Acta*, 69(11), 2745–2752, doi:10.1016/j.gca.2004.11.026, 2005.

68 Swart, S., Speich, S., Ansorge, I. J. and Lutjeharms, J. R. E.: An altimetry-based gravest empirical mode south of Africa: 1.
69 Development and validation, *J. Geophys. Res. Ocean.*, 115(3), 1–19, doi:10.1029/2009JC005299, 2010.

70 Takahashi, T., Sweeney, C., Hales, B., Chipman, D. W., Goddard, J. G., Newberger, T., Iannuzzi, R. A. and Sutherland, S. C.:
71 The changing carbon cycle in the southern ocean, *Oceanography*, 25(3), 26–37, doi:10.5670/oceanog.2012.71, 2012.

72 Taylor, S. R. and McLennan, S. M.: The continental crust: Its composition and evolution, Blackwell Scientific Pub., Palo Alto,
73 CA, United States. [online] Available from: <https://www.osti.gov/biblio/6582885>, 1985.

74 Thomalla, S. J., Fauchereau, N., Swart, S. and Monteiro, P. M. S.: Regional scale characteristics of the seasonal cycle of
75 chlorophyll in the Southern Ocean, *Biogeosciences*, 8(10), 2849–2866, doi:10.5194/bg-8-2849-2011, 2011.

76 Trull, T. W., Passmore, A., Davies, D. M., Smit, T., Berry, K. and Tilbrook, B.: Distribution of planktonic biogenic carbonate
77 organisms in the Southern Ocean south of Australia: A baseline for ocean acidification impact assessment, *Biogeosciences*,
78 15(1), 31–49, doi:10.5194/bg-15-31-2018, 2018.

79 Twining, B. S., Nodder, S. D., King, A. L., Hutchins, D. A., LeCleir, G. R., DeBruyn, J. M., Maas, E. W., Vogt, S., Wilhelm,
80 S. W. and Boyd, P. W.: Differential remineralization of major and trace elements in sinking diatoms, *Limnol. Oceanogr.*,
81 59(3), 689–704, doi:<https://doi.org/10.4319/lo.2014.59.3.0689>, 2014.

82 van Beek, P., François, R., Conte, M., Reyss, J. L., Souhaut, M. and Charette, M.: $^{228}\text{Ra}/^{226}\text{Ra}$ and $^{226}\text{Ra}/\text{Ba}$ ratios to track
83 barite formation and transport in the water column, *Geochim. Cosmochim. Acta*, 71(1), 71–86,
84 doi:10.1016/j.gca.2006.07.041, 2007.

85 Viljoen, J. J., Philibert, R., Van Horsten, N., Mtshali, T., Roychoudhury, A. N., Thomalla, S. and Fietz, S.: Phytoplankton
86 response in growth, photophysiology and community structure to iron and light in the Polar Frontal Zone and Antarctic
87 waters, *Deep. Res. Part I Oceanogr. Res. Pap.*, 141(September), 118–129, doi:10.1016/j.dsr.2018.09.006, 2018.

88 Wright, S. W., van den Enden, R. L., Pearce, I., Davidson, A. T., Scott, F. J. and Westwood, K. J.: Phytoplankton community
89 structure and stocks in the Southern Ocean (30–80°E) determined by CHEMTAX analysis of HPLC pigment signatures,
90 *Deep. Res. Part II Top. Stud. Oceanogr.*, 57(9–10), 758–778, doi:10.1016/j.dsr2.2009.06.015, 2010.

91 Zhuang, J.: xESMF: Universal Regridder for GeospatialData, <https://github.com/JiaweiZhuang/xESMF>, 2018.

92